Architecture-Driven Level Set Optimization: From Clustering to Subpixel Image Segmentation

Souleymane Balla-Arabé, *Member, IEEE*, Xinbo Gao, *Senior Member, IEEE*, Dominique Ginhac, *Member, IEEE*, Vincent Brost, and Fan Yang

***Abstract*—Thanks to their effectiveness, active contour models (ACMs) are of great interest for computer vision scientists. The level set methods (LSMs) refer to the class of geometric active contours. Comparing with the other ACMs, in addition to subpixel accuracy, it has the intrinsic ability to automatically handle topological changes. Nevertheless, the LSMs are computationally expensive. A solution for their time consumption problem can be hardware acceleration using some massively parallel devices such as graphics processing units (GPUs). But the question is: which accuracy can we reach while still maintaining an adequate algorithm to massively parallel architecture? In this paper, we attempt to push back the compromise between, speed and accuracy, efficiency and effectiveness, to a higher level, comparing with state-of-the-art methods. To this end, we designed a novel architecture-aware hybrid central processing unit (CPU)–GPU LSM for image segmentation. The initialization step, using the well-known *k*-means algorithm, is fast although executed on a CPU, while the evolution equation of the active contour is inherently local and therefore suitable for GPU-based acceleration. The incorporation of local statistics in the level set evolution allowed our model to detect new boundaries which are not extracted by the used clustering algorithm. Comparing with some cutting-edge LSMs, the introduced model is faster, more accurate, less subject to giving local minima, and therefore suitable for automatic systems. Furthermore, it allows two-phase clustering algorithms to benefit from the numerous LSM advantages such as the ability to achieve robust and subpixel accurate segmentation results with smooth and closed contours. Intensive experiments demonstrate, objectively and subjectively, the good performance of the introduced framework both in terms of speed and accuracy.**

***Index Terms*—Graphics processing units (GPUs), hybrid CPU–GPU architecture, image segmentation, level set method (LSM).**

Manuscript received April 3, 2015; revised June 11, 2015, August 16, 2015, and October 21, 2015; accepted October 30, 2015. This work was supported in part by the Regional Council of Burgundy (Conseil Régional de Bourgogne, France), in part by the National Natural Science Foundation of China under Grant 61125204 and Grant 61432014, in part by the Fundamental Research Funds through the Central Universities under Grant BDZ021403 and Grant JB149901, in part by the Program for Changjiang Scholars and Innovative Research Team in the University of China under Grant IRT13088, and in part by the Shaanxi Innovative Research Team for Key Science and Technology under Grant 2012KCT-02. This paper was recommended by Associate Editor D. Goldgof.

S. Balla-Arabé, D. Ginhac, V. Brost, and F. Yang are with the Laboratory of Electronic, Computing and Imaging Sciences CNRS-UMR 6306, University of Burgundy, Dijon 21078, France (e-mail: balla_arabe_souleymane@ieee.org; dom@le2i.cnrs.fr; vincent.brost@free.fr; fanyang@u-bourgogne.fr).

X. Gao is with the State Key Laboratory of Integrated Services Networks, School of Electronic Engineering, Xidian University, Xi'an 710071, China (e-mail: xbgao@mail.xidian.edu.cn).

Color versions of one or more of the figures in this paper are available online at http://ieeexplore.ieee.org.

Digital Object Identifier 10.1109/TCYB.2015.2499206

I. Introduction

In COMPUTER vision and pattern recognition, image segmentation [1]–[7] is a major process by which a given image is partitioned into a number of meaningful and homogeneous regions, such that the union of any two neighborhood regions yields a heterogeneous segment. Due to the fact that there is no a general framework which is effective for all kinds of images, the task is nontrivial and more challenging in presence of noise. One should choose the proper method according to the characteristics of the image in hand.

In recent years, optimization methods have attracted much attention as powerful and natural image segmentation tools. Their basic principle is to achieve segmentation by minimizing a given energy function designed from the image information. Optimization methods can be roughly classified into two important classes: 1) spatially discrete and 2) spatially continuous representations. In spatially discrete approaches, the image pixels are usually considered as the nodes of a graph, and the aim of segmentation is to find cuts of this graph which have a minimal cost [8], [9].

Active contour models (ACMs) belong to the spatially continuous approaches: the segmentation of the image plane is considered as a problem of infinite-dimensional optimization. The main idea is to evolve a given curve in the direction of negative energy gradient by means of an appropriate partial differential equation. The level set method (LSM) [10]–[13] designates the class of ACMs which uses the Eulerian framework, i.e., the geometric representation of the evolving curve, instead of the parametric one, i.e., the Lagrangian framework [14]–[17]. Fig. 1 displays the organization of the ACMs.

Comparing with parametric active contours, the LSM presents more advantages, such as the ability to easily handle complex shapes, and topological changes. Furthermore, it allows a straightforward passage from 2-D to 3-D space. The original idea of the LSM stems from the Hamilton Jacobi approach, i.e., a time-dependent equation for a moving surface [18]–[20]. In space, the LSM aims to evolve a given curve toward its interior or exterior normal until defining the boundary of the object of interest. The curve evolution is driven by the level set equation (LSE) which is a nonlinear

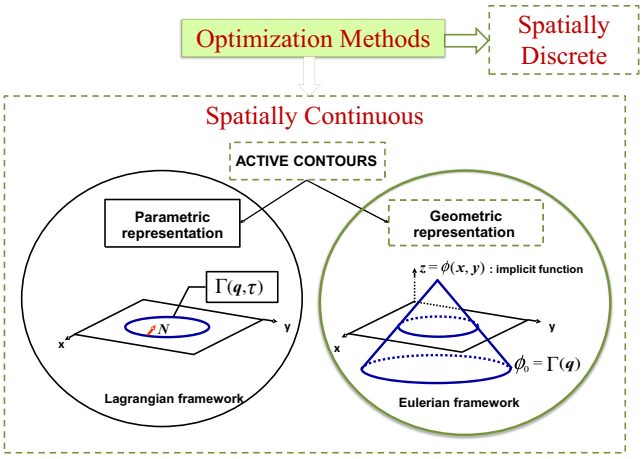

Fig. 1. Organization ACMs.

partial differential equation formulated as follows:

$$\frac{\partial \phi}{\partial t} = \|\nabla \phi\|(\mu V + \varepsilon k) \tag{1}$$

where ϕ is the level set function (LSF), V the velocity field which guides the active curve toward the needed boundaries, μ and ε are user-controlling parameters, and k is a nonlinear curvature term expressed as

$$k = \nabla \cdot \left(\nabla \phi / \|\nabla \phi\|\right). \tag{2}$$

Two main approaches are usually used to stop the evolving curve on the contours of the desired object. The first uses an edge indicator depending on the gradient of the image, as in classical snake and ACMs [21]–[25]. These models have a lower computational complexity and are suitable to parallel architecture, but they are sensitive to noise and initialization.

The second uses some regional attributes to stop the evolving curve on the real boundary. These models are more robust against noise and can detect objects with weak edges. One of the most known region-based level set algorithms was proposed in [29], where Chan and Vese introduced a level set formulation to minimize the Mumford and Shah [30] functional. They converted the problem into a mean curvature flow problem just like the active contours. Karantzalos and Argiala [27] used this approach in the field of remote sensing imagery for automatic detection of man-made objects (roads, buildings, etc.) from aerial and satellite images. Bazi *et al.* [52] presented an unsupervised change detection method for multispectral images by designing a region-based energy functional using the difference image. The level set framework was then used to minimize the designed functional.

The region-based level set algorithms give better results than those of the classical active contours because the stopping term did not depend on the gradient of the image, reducing the dependence on strong edges, and improving the robustness against noise. However, most of the times they cannot deal with intensity inhomogeneities, and are definitely not suitable for parallel programming, because they are not local. Furthermore, in order to solve the LSE, most of these methods suggest the use of some computationally expensive finite difference, finite element, or finite volume approximations and an explicit computation of the curvature [31], [32].

In our previous work [26], [28], in order to handle the problem of computational expense, we used the lattice Boltzmann method (LBM) as an alternative approach for solving the LSE. Comparing with [29] for example, these approaches give better results in terms of efficiency and accuracy. The problem of time consumption is better handled because the curvature is implicitly computed and the algorithm is simple. But these introduced methods have some limits. In [26], we used regional attributes of a given pixel to design an unsigned pressure force (UPF) which acted as a stop function for the active curve. This method is greatly dependent to the initialization which limits its use in automatic systems. Furthermore, the UPF is not local and therefore not suitable to parallel architecture-based acceleration. In [28], we used both local and regional statistics to design an energy function which had to be minimized using the level set framework, the method was more effective and robust against initialization than the one introduced in [26]. But as in [28], we still need to compute the mean values of pixels intensity inside and outside the active curve at each iteration, which increases the communication between the processors of any massively parallel device like graphics processing unit (GPU), and therefore slowdown the method.

In this paper, we introduce a novel architecture-driven framework which allows obtaining a highly effective and fully local LSE. Therefore, the proposed algorithm is adequate to parallel hardware-based acceleration, while allowing the achievement of promising segmentation results. In addition, the proposed method is a general framework which allows to considerably improving the results of most two-phase clustering methods such as k-means, the fuzzy c-means (FCM) and their derivatives. By using the two intensity means output of the clustering algorithms and some local statistics of the image, we design an effective and inherently local energy functional. A fully local LSE is then obtained using the gradient descent methods. This strategy effectively allows combining, in a straightforward manner, the advantages of clustering techniques and LSMs. On the one hand, the speed and the low complexity of some clustering algorithms, such as k-means, make the methods faster in comparison to some state of the art LSMs; on the other hand, the method has the advantages of the LSMs such as the ability to:

1) achieve subpixel accuracy [29];
2) allow the incorporation of various prior knowledge, for example, shape and intensity distribution in order to achieve more robust segmentation results [33];
3) provide smooth and closed contours which are ineluctable for further applications such as shape analysis and recognition [34].

Although, most of two-phase clustering methods can be used, in this paper, we use the output of the k-means algorithm, which has been initialized using the interior and the exterior intensity means of the initial active curve. The k-means algorithm, which is intrinsically fast and nonlocal, is executed on the central processing unit (CPU), while the level set evolution

is executed on an NVIDIA GPU. The major contributions of the present paper can be summarized as follows.

1) A novel inherently local and effective level set framework which perfectly suited to massively parallel architecture. The method can therefore be used in real-time computer vision systems.
2) A novel technique allowing some original clustering methods to benefit from the LSMs numerous advantages, and vice versa.
3) The introduction of local statistics in the level set evolution equation allowing the detection of new boundaries which are not extracted by the clustering algorithm. As a result:
   a) the minimization framework is less subject to giving local minima;
   b) the framework is therefore less sensitive to initialization than the classical LSM and the k-means algorithm taken alone;
   c) the algorithm suits more to automatic systems.
4) A robust and effective hybrid CPU–GPU framework for fast image segmentation.

Intensive experiments, using the Berkeley segmentation dataset BSDS300 [35], demonstrate, subjectively and objectively, the effectiveness and efficiency of the proposed segmentation framework.

The remainder of the paper is organized as follows. Section II introduces the LBM. The formulation of the proposed method is given in Section III. Section IV presents the experimental results. The final section is the conclusion.

II. Background

This section gives a general idea of the lattice Boltzmann model. The LBM was first designed to simulate Navier–Stokes equations for an incompressible fluid [37]–[39]. Its evolution equation is

$$f_i(\vec{r}+\vec{e}_i, t+1) = f_i(\vec{r}, t) + \left(\frac{\partial f}{\partial t}\right)_{\text{coll}} \tag{3}$$

which can be decomposed into two steps

$$\text{collision: } f^{\text{coll}}(\vec{r}, t) = f_i(\vec{r}, t) + \left(\frac{\partial f}{\partial t}\right)_{\text{coll}} \tag{4}$$

$$\text{streaming: } f_i(\vec{r}+\vec{e}_i, t+1) = f^{\text{coll}}(\vec{r}, t) \tag{5}$$

where f_i is the particle distribution function and $\vec{r}$ is a spatial variable. In this paper, $\left(\partial f/\partial t\right)_{\text{coll}}$ is the Bhatnager–Gross–Krook collision model [40]–[43], with a body force $\vec{F}$, expressed as

$$\left(\frac{\partial f}{\partial t}\right)_{\text{coll}} = \frac{1}{\tau}\cdot\left[f_i^{\text{eq}}(\vec{r}, t) - f_i(\vec{r}, t)\right] + \frac{D}{bc^2}\cdot\vec{F}.\vec{e}_i \tag{6}$$

where D is the grid dimension, b is the link number at each grid point, c is the length of each link which is set to 1 in this paper, and τ represents the relaxation time. f_i^{eq} is the local Maxwell–Boltzmann equilibrium particle distribution function expressed in its continuous form as

$$f_{\text{eq}} = \rho(2\pi\text{RT})^{-3/2}\exp\left\{-\frac{(\vec{v}-\vec{u})^2}{2\text{RT}}\right\} \tag{7}$$

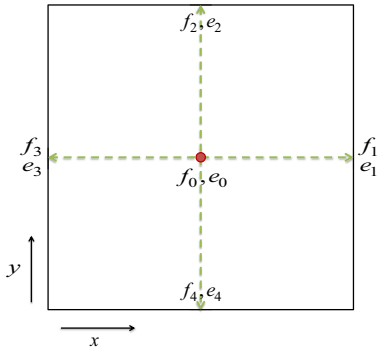

Fig. 2. Spatial structure of the D2Q5 LBM lattice.

where $\vec{v}$ is the particle velocity and $\vec{u}$ is the macroscopic velocity. The equilibrium distribution can be expressed in discrete form as follows when modeling typical diffusion phenomenon:

$$f_i^{\text{eq}}(\rho) = \rho A_i \text{ with } \rho = \sum_i f_i \tag{8}$$

where ρ is the macroscopic fluid density. By performing the Chapman–Enskog expansion [44], the following diffusion equation can be recovered from the lattice Boltzmann evolution equation [38]:

$$\frac{\partial \rho}{\partial t} = \beta\text{div}(\nabla\rho) + F. \tag{9}$$

Substituting ρ by the signed distance function ϕ in (9), the LSE can be recovered. In our model we use the D2Q5 ($D = 2$, $b = 5$) LBM lattice structure. Fig. 2 displays a typical D2Q5 model where each link has its velocity vector $e_i(\vec{r}, t)$. The body force F acts as the link with image data for the LBM solver.

Reference [45] used another approach to perform the level set image segmentation. Equation (3) is the general evolution equation of the LBM; however, in level-set-based image segmentation, a stop function $g_i(\vec{r})$ is necessary to stop the evolving curve or surface at the boundaries of the object. In order to introduce the stop function into the LBM, the authors considered a medium between the nodes of the lattice. The particles can pass through the medium with a possibility of $g_i(\vec{r})$, and will be pushed back to where they were with a possibility of $1 - g_i(\vec{r})$. The LBM evolution equation is modified as

$$f_i(\vec{r}+\vec{e}_i, t+1) = g_i(\vec{r})\left[f(\vec{r}, t) + \frac{1}{\tau}\left[f_i^{\text{eq}}(\vec{r}, t) - f_i(\vec{r}, t)\right]\right] + \sigma + (1 - g_i(\vec{r}))f_i(\vec{r}+\vec{e}, t) \tag{10}$$

where σ is the convection coefficient. The macroscopic fluid density ρ is set as a signed distance function. More details about this approach can be found in [45].

III. Proposed Hybrid Level Set Framework for Two-Phase Image Segmentation

This section is dedicated to the conception and analysis of the proposed algorithm. We first design a novel energy functional, which will be minimized using the level set framework.

Let $\phi : \Omega \to \mathbb{R}$ be an LSF defined on a domain Ω. In all our work, ϕ is a signed distance function positive inside the zero level contour Γ and positive outside. The introduced energy functional is defined as follows:

$$E(\phi) = E_{\text{main}}(\phi) + E_{\text{Regularization}}(\phi) \tag{11}$$

where $E_{\text{main}}(\phi)$ is the main energy term which contains the regional information of the image to be segmented, $E_{\text{Regularization}}(\phi)$ is the constraint on the smoothness and the length of the evolving contour.

By using the gradient descent method, the LSE can be recovered from the above defined energy function

$$\frac{\partial \phi}{\partial t} = \frac{\partial E}{\partial \phi} \tag{12}$$

where $\partial E/\partial \phi$ is the Gâteaux derivative [46] of ε. According to (11) and (12) is equivalent to the following evolution equation:

$$\frac{\partial \phi}{\partial t} = -\frac{\partial E_{\text{main}}(\phi)}{\partial \phi} - \frac{\partial E_{\text{Regularization}}(\phi)}{\partial \phi}. \tag{13}$$

A. Design of $E_{main}(\phi)$

The main energy term $E_{\text{main}}(\phi)$ has been designed so that:

1) it is inherently local in order to suit to massively parallel architecture;
2) its minimization yields to an effective and accurate image segmentation even in the presence of outliers.

$E_{\text{main}}(\phi)$ is therefore defined as

$$\begin{aligned} E_{\text{main}}(\phi) = {} & \gamma \int_{\Omega} \left(1 - \exp\left\{-\left(I(x) - P_1/\omega_1\right)^2\right\}\right) H(\phi) dx \\ & + \lambda \int_{\Omega} \left(1 - \exp\left\{-\left(I(x) - P_2/\omega_2\right)^2\right\}\right) \\ & (1 - H(\phi)) dx \\ & + E_{\text{Outliers}}(\phi) \end{aligned} \tag{14}$$

where E_{Outliers} is the energy to be minimized in order to make the method robust against outliers, H is the Heaviside function, x is a spatial variable, γ and λ are the user controlling positive constants, ω_1 and ω_2 are the important parameters which can lead, if wrongly chosen, to an over or under segmentation result. In this paper, we used $\omega_1 = \omega_2 = 1$. The values of P_1 and P_2 are obtained as follows. The interior and the exterior intensity average of the initial active curve are used to initialize a two-phase k-means algorithm, P_1 and P_2 are the mean values of the two final classes obtained. This part constitutes the serial part of our algorithm, and it is fast since computational efficiency is one of the main advantages of the k-means algorithm.

The derivative of $E_{\text{main}}(\phi)$ with respect to ϕ can therefore be formulated as

$$\begin{aligned} \frac{\partial E_{\text{main}}}{\partial \phi} = {} & \delta(\phi)\Big[\gamma\left(1 - \exp\left\{-\left(I(x) - P_{\text{in}}/\omega_1\right)^2\right\}\right) \\ & - \lambda\left(1 - \exp\left\{-\left(I(x) - P_{\text{out}}/\omega_2\right)^2\right\}\right)\Big] + \frac{\partial E_{\text{Outliers}}}{\partial \phi}. \end{aligned} \tag{15}$$

In [26], we had defined an efficient energy term based on a 2-D gray-scale histogram which can make the LSM more robust by avoiding the evolving curve stopping at the pixels which are more likely to be outliers. This energy term was defined as follows:

$$\begin{aligned} \varepsilon_{\text{2D-hist}}(\phi) = {} & \int_{\Omega} (\alpha m_1 + \beta m_2 - I) \\ & \times \exp\{\mu(|I - I_{\text{mean}}| - \eta)\} H(\phi) dxdy \end{aligned} \tag{16}$$

where I_{mean} represents the local average, α and β are the user-controlling parameters, η and μ are the positive constants, m_1 and m_2 are, respectively, the mean intensity values inside and outside the active contour and have to be computed at each iteration as follows:

$$m_1 = \int_{\Omega} I(x, y) \cdot H(\phi) dxdy \Big/ \int H(\phi) dxdy \tag{17}$$

$$m_2 = \int_{\Omega} I(x, y) \cdot (1 - H(\phi)) dxdy \Big/ \int H(\phi) dxdy. \tag{18}$$

In this paper, inspired by the energy term defined in (16), we define E_{Outliers} as follows:

$$\begin{aligned} & E_{\text{Outliers}}(\phi) = A(P_1, P_2) \int_{\Omega} \exp\{\mu(|I - I_{\text{mean}}| - \eta)\} H(\phi) dx \\ & \text{with } A(P_1, P_2) = \gamma\left(1 - \exp\left\{-(I(x) - P_1/\omega_1)^2\right\}\right) \\ & \qquad - \lambda\left(1 - \exp\left\{-(I(x) - P_2/\omega_2)^2\right\}\right). \end{aligned} \tag{19}$$

A straightforward analysis of E_{Outliers} shows that the effect of it minimization is to make the present method robust against outliers by avoiding the evolving curve stopping at pixels for which the intensity value is far different from their local intensity average, that is, high gradient isolate pixels. The derivative of E_{Outliers} with respect to ϕ can therefore be written as follows:

$$\frac{\partial E_{\text{Outliers}}}{\partial \phi} = [A(P_1, P_2) \exp\{\mu(|I - I_{\text{mean}}| - \eta)\}] \delta(\phi). \tag{20}$$

By adding this term in the main energy, we finally get the following equation:

$$\frac{\partial E_{\text{main}}}{\partial \phi} = \delta(\phi) A(P_1, P_2)[1 + \exp\{\mu(|I - I_{\text{mean}}| - \eta)\}]. \tag{21}$$

B. Design of $E_{Regularization}(\phi)$

In traditional LSM, the regulation term used as a constraint on the area and the length of the active contour [29] is expressed as

$$\begin{aligned} E(\phi) &= E_{\text{Area}}(\phi) + E_{\text{Length}}(\phi) \\ &= \vartheta \int_{\Omega} H(\phi) dx + \nu \int_{\Omega} \|\nabla H(\phi)\| dx \end{aligned} \tag{22}$$

where ϑ and ν are user controlling parameters. Its derivative with respect to ϕ is expressed as

$$\begin{aligned} \frac{\partial E}{\partial \phi} &= \frac{\partial E_{\text{Area}}}{\partial \phi} + \frac{\partial E_{\text{Length}}}{\partial \phi} \\ &= \vartheta \delta(\phi) - \nu \text{div}(\nabla \phi / \|\nabla \phi\|) \delta(\phi). \end{aligned} \tag{23}$$

In this paper, we introduced a local statistics-based constraint in the classical regularization term. Therefore, the modified regularization term is expressed as follows:

$$E_{\text{Regularization}}(\phi) = \vartheta \int_{\Omega} H(\phi)dx + \nu \int_{\Omega} \nabla H(\phi)dx + C(\phi)$$
$$\text{with } C(\phi) = \sigma \text{sign}(\nabla I)H(\varepsilon - \exp\{\|\nabla I\|\}) \int_{\Omega}(1 - H(\phi))dx \quad (24)$$

where σ and ε are positive parameters. The term $C(\phi)$ is designed in order to attract the evolving curve toward the sectors of the image domain where the gradient is medium or high. Since the LSF ϕ is defined so that it is positive inside the zero level contour and positive outside. A straightforward analysis of $C(\phi)$ leads to the following conclusion:

1) $\phi \geq 0 \Rightarrow C(\phi) = 0$;
2) $\phi < 0 \Rightarrow \begin{cases} \text{if} \exp\{\|\nabla I\|\} < \varepsilon \Rightarrow C(\phi) = \sigma \text{sign}(\nabla I) \\ \text{if} \exp\{\|\nabla I\|\} > \varepsilon \Rightarrow C(\phi) = 0. \end{cases}$

We can therefore notice that when the curve is evolving, $C(\phi)$ is different from zero and has the sign of ∇I when the curve is on a pixel for which $\exp\{\|\nabla I\|\} < \varepsilon$. This makes the curve expands or contracts in order to evolve toward higher gradient pixels.

But since $E_{\text{main}}(\phi)$ is designed so that the evolving curve cannot stop on high gradient pixels, in order to make the proposed model robust against outliers, the designed regularization term will increase the ability to detect objects delineated by medium edges and weak edges depending on the threshold parameter ε. The derivative of the proposed regularization term with respect to ϕ can be written as follows:

$$\frac{\partial E_{\text{Regularization}}}{\partial \phi} = \delta(\phi)[\vartheta - \nu \text{div}\left(\nabla\phi / \|\nabla\phi\|\right) - \sigma \text{sign}(\nabla I)H(\varepsilon - \exp\{\|\nabla I\|\})]. \quad (25)$$

Finally, we obtain the following LSE:

$$\frac{\partial \phi}{\partial t} = -\delta(\phi)(A(P_1, P_2)[1 + \exp\{\mu(|I - I_{\text{mean}}| - \eta)\}] + \vartheta - \nu \text{div}\left(\nabla\phi / \|\nabla\phi\|\right) - \sigma \text{sign}(\nabla I) H(\varepsilon - \exp\{\|\nabla I\|\})) \quad (26)$$

with

$$A(P_1, P_2) = \gamma\left(1 - \exp\left\{-\left(I(x) - P_1/\omega_1\right)^2\right\}\right) - \lambda\left(1 - \exp\left\{-\left(I(x) - P_2/\omega_2\right)^2\right\}\right).$$

In order to extend the evolution to all the level set of ϕ, the gradient projection method [47] allows us to replace $\delta(\phi)$ by $\|\nabla\phi\|$. To maintain the suitability to parallel programming of our model, we use the local LBM to solve the obtained LSE. By setting ϕ as a signed distance function, that is, $\|\nabla\phi\| = 1$, and constraining it to stay like that, (26) can be written as follows:

$$\frac{\partial \phi}{\partial t} = -A(P_1, P_2)[1 + \exp\{\mu(|I - I_{\text{mean}}| - \eta)\}] - \vartheta + \sigma \text{sign}(\nabla I)H(\varepsilon - \exp\{\|\nabla I\|\}) + \nu \text{div}(\nabla\phi) \quad (27)$$

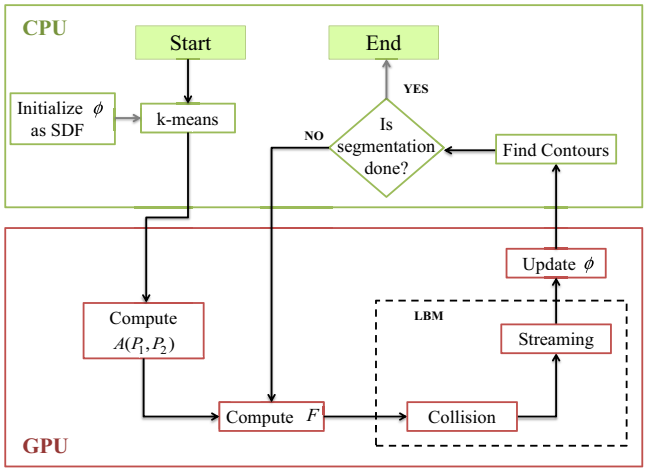

Fig. 3. Flowchart representing the process of the proposed algorithm.

Algorithm 1 Main stages of the proposed algorithm

Input: Initial zero level contour ϕ (signed distance function), ε, η, γ, λ, μ, ϑ and σ.

Output: The final zero LSF contours ϕ.

Algorithm Steps:

1. Run the k-means algorithm with the interior and exterior means of the initial active curve as initial values.
2. Compute the body force F with Eq. (28).
3. Resolve the LSE using LBM with Eq. (29).
4. Accumulate the $f_i(\vec{r}, t)$ values at each grid point with Eq. (8), which generates updated values of ϕ.
5. Find the contours (zero level contours of the LSF).
6. If the algorithm has not converged, i.e., $\left\|\phi^{t+1} - \phi^t\right\| > 10^{-5}$, go back to step 3.

which is similar to (9) with the body force expressed as

$$F = -A(P_1, P_2)[1 + \exp\{\mu(|I - I_{\text{mean}}| - \eta)\}] - \vartheta + \sigma \text{sign}(\nabla I)H(\varepsilon - \exp\{\|\nabla I\|\}). \quad (28)$$

The proposed LSE can therefore be solved using the following lattice Boltzmann evolution equation:

$$f_i(\vec{r} + \vec{e}_i, t + 1) = f_i(\vec{r}, t) + (1/\tau) \cdot \left[f_i^{\text{eq}}(\vec{r}, t) - f_i(\vec{r}, t)\right] + \left(D/bc^2\right)(-A(P_1, P_2)[1 + \exp\{\mu(|I - I_{\text{mean}}| - \eta)\}] - \vartheta + \sigma \text{sign}(\nabla I)H(\varepsilon - \exp\{\|\nabla I\|\})) \quad (29)$$

without the necessity to explicitly calculate the computational expansive curvature term since it is implicitly handled by LBM.

Fig. 3 illustrates the flowchart of the proposed level set-based algorithm, where we can clearly distinguish which part is executed on the CPU and which one on the GPU.

The principal implementation steps of the proposed method are given in Algorithm 1.

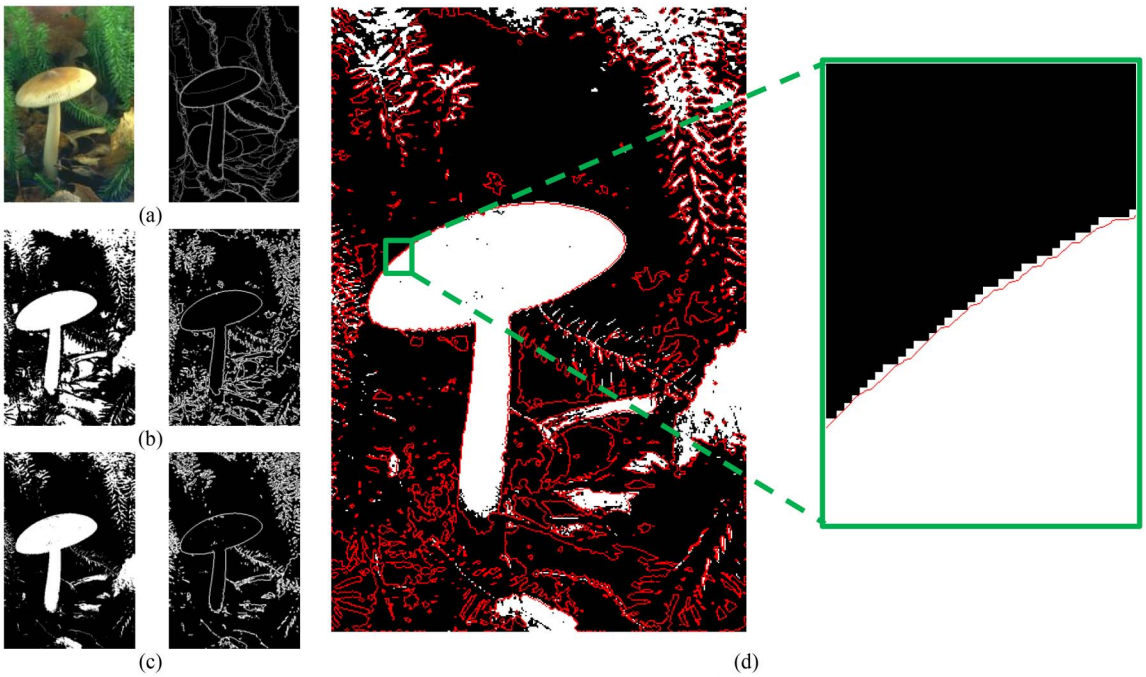

Fig. 4. (a) Natural image with human segmentation as ground truth. Segmentation result of the (b) proposed algorithm, binary, and contour representations and (c) k-means algorithm, binary, and contour representations. (d) Superimposition of the k-means result with the contours (in red) extracted by the method introduced in this paper.

IV. Experimental Results and Analysis

This section demonstrates the performance of the proposed architecture-driven level set image segmentation method [architecture-driven level set optimization (A-DLSO)] both in terms of efficiency and effectiveness.

A. Experimental Setup

The experiments environment is the parallel computing toolbox of MATLAB R2013a installed on a laptop Aspire V3-571G with an Intel Core i3-2348M (2.3 GHz, 3 MB L3 cache) processor and possessing a GPU NVIDIA GeForce 710M with 2 GB dedicated VRAM. The executive time in all the experiments invoking the graphics card includes the transfer time of data from the CPU to the graphics card and vice versa. In this paper, we have empirically set the parameters. In all the experiments, the chosen parameters are those who give the highest F-measure average. For our model, we fixed $\varepsilon = 0.01$, $\eta = 0.2$, $\gamma = 5$, $\lambda = 5$, $\mu = 2$, $\vartheta = 0$, and $\sigma = 5$.

The optimized MATLAB function arrayfun is used to execute the A-DLSO, the CV, and the HZ code on the GPU. For example, the body force of the A-DLSO is computed using the following instructions.

1) Id = gpuArray(I).
2) Imean$d$ = gpuArray(Imean).
3) Fd = arrayfun(@Body_force,Id,Imean$d$).

The first and the second instruction transfer, respectively, I and I_{mean} from the CPU to the GPU, while the third instruction computes the body force on the GPU using the kernel function Body_force.m programmed according to (28). Since all the output arguments are stored in the GPU memory, the function gather is used to transfer them back from GPU to CPU.

To best use the GPU capability, we restructure our code in order to maximally reduce the number of loops by using code vectorization technique. A good explanation of this method can be found in MATLAB online support.

In this paper, the GPU task and thread assignments are automatically handled by MATLAB. Nevertheless, we should notice that the introduced model could be considerably faster by using the compute unified device architecture (CUDA) framework with our own task and thread management strategies. Furthermore, since the curve evolution is fully local, the use of CUDA kernels can provide a big speed-up, for example, the collision step of the LBM can be a good candidate.

The supervised objective evaluation is undertaken using the F-measure based on precision and recall. It measures the similarity between two images. The higher it is, the better the segmentation result. It is formulated as follows [48], [49]:

$$\begin{aligned} F &= \left[\left(1+\rho^2\right)\cdot R\cdot P\right]/\left(\rho^2\cdot R + P\right) \\ \text{with } R &= \text{True Positive}/(\text{True Positive} + \text{False Negative}) \\ \text{and } P &= \text{True Positive}/(\text{True Positive} + \text{False Positive}) \end{aligned} \tag{30}$$

where R and P are, respectively, recall and precision, ρ is usually set to 1.

In order to better allow the subjective evaluation, we presented the results of all the methods that we used in two forms: 1) by binary images and 2) by only contours. To obtain the binary representation, the interior of the obtained contour is represented by white pixels and the exterior by black pixels. The blue triangle is the initial contour. The dimensions used are 450×948, with the exception of Fig. 4, where the dimensions of the image are of 948×450.

The proposed method and all the methods used for comparison were run using the intensity information I of color

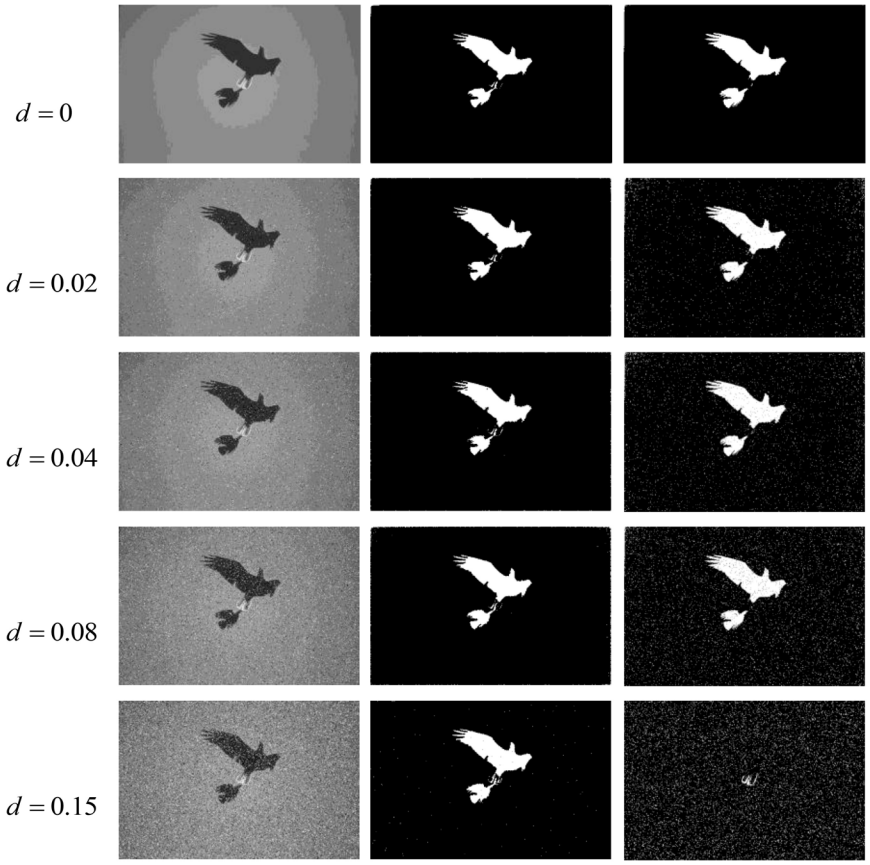

Fig. 5. Segmentation of an image corrupted by salt and pepper noise with different density values d. The first column displays the corrupted images. The second column presents the results of the proposed method. The third column presents the results of the k-means algorithm.

TABLE I
STATISTICAL RESULTS OF THE OBJECTIVE EVALUATION USING F-MEASURE (%)

Methods	Average	Standard deviation
A-DLSO	90.7841	0.9028
CV	78.0608	2.7437
HZ	76.1850	1.5957
k-means	79.0566	1.0073
FCM	79.9786	0.8641
PKGC	83.1696	0.8743
Li	81.7851	1.9599
GF	78.1173	1.6935

images, which was obtained by performing a weighted sum of the R, G, and B components as recommended by the 601 resolution of the International Commission on Illumination

$$I = 0.2989 \cdot R + 0.5870 \cdot G + 0.1140 \cdot B. \tag{31}$$

B. Experimental Results

In this section, we compare the introduced framework with the following methods.

1) The recent parametric kernel graph cuts (PKGCs)-based image segmentation method introduced by Salah *et al.* [50].
2) The region-based ACM (CV) introduced by Chan and Vese [29].
3) The two-phase FCM clustering method.
4) The two-phase k-means clustering algorithm.
5) The local ACM (HZ) introduced by Hagan and Zhao [51].
6) The ACM for image segmentation in the presence of intensity inhomogeneities introduced by Li *et al.* [13].
7) The fast ACM (GF) described by Gibou and Fedkiw [36].

Fig. 4 gives evidence of the way the proposed method improves clustering algorithms by allowing them to achieve subpixel accurate segmentation with smooth and closed contours. In this paper, we used the mean values of the two final classes obtained by the k-means algorithm. Nevertheless, another clustering algorithm, such as the FCM or support vector machine (SVM), can be used. Fig. 4(a) displays the original image with human segmentation as ground truth. As we can see from Fig. 4(b) and (c), more useful contours are detected by our model. In Fig. 4(d), we superimposed the k-means segmentation result with the final level set contour of the proposed algorithm represented in red. We can see that the contour is closed, smoother, and the F-measure, comparing the result with human segmentation, gives a score of 89.95% for our introduced framework and only 77.09% for the k-means. Thus, the result obtained by our model is far

Fig. 6. Segmentation of real-world images. The first row presents the original images with the initial contour, and the corresponding human segmentation as ground truth. The second row presents the results of the proposed algorithm. The third row presents the results of the *k*-means clustering method. The fourth row presents the results of the FCM clustering method. The fifth row presents the results of the PKGC method. The sixth row presents the results of the CV method. The seventh row presents the results of the HZ method. The eighth row presents the results of the Li method. The last row presents the results of the GF method. For all the methods, the results are presented in two ways, i.e., by contours and binary images.

better in term of accuracy. This is an ineluctable proof on how it can greatly improve the quality performance of two-phase clustering algorithms.

Fig. 5 demonstrates the robustness of the proposed method against outliers. In this experiment, we simulated outliers using salt and pepper noise with different density values. The comparison with the *k*-means algorithm clearly shows the superiority of the proposed framework. The last row shows that even if the *k*-means fails, the A-DLSO is able to achieve a pretty good segmentation thanks to the use of local statistics, and the constraints on the area and the length introduced during the curve evolution.

Fig. 7. Segmentation of real-world images. The first row presents the original images with the initial contour, and the corresponding human segmentation as ground truth. The second row presents the results of the proposed algorithm. The third row presents the results of the *k*-means clustering method. The fourth row presents the results of the FCM clustering method. The fifth row presents the results of the PKGC method. The sixth row presents the results of the CV method. The seventh row presents the results of the HZ method. The eighth row presents the results of the Li method. The last row presents the results of the GF method. For all the methods, the results are presented in two ways, i.e., by contours and binary images.

From Figs. 6–8, we challenged the proposed algorithm using the PKGC, the CV, the FCM, the *k*-means, the HZ, the Li, and the GF methods. The results of the supervised objective evaluation are displayed in Table I and the 3-D histogram of Fig. 9. The executive times of the serial implementation on the CPU of all the algorithms used in this section are presented in Table II. Finally, the executive times of the GPU-based implementation of the A-DLSO, CV, and HZ are displayed in Table III.

According to Table I, it can be seen that in almost all the experiments the proposed algorithm has the highest average *F*-measure, i.e., the produced result is the closest to

Fig. 8. Segmentation of real-world images. The first row presents the original images with the initial contour, and the corresponding human segmentation as ground truth. The second row presents the results of the proposed algorithm. The third row presents the results of the *k*-means clustering method. The fourth row presents the results of the FCM clustering method. The fifth row presents the results of the PKGC method. The sixth row presents the results of the CV method. The seventh row presents the results of the HZ method. The eighth row presents the results of the Li method. The last row presents the results of the GF method. For all the methods, the results are presented in two ways, i.e., by contours and binary images.

human segmentation used as ground-truth. The subjective evaluation also confirms the superiority of the our model since it extracted more useful, thin, and nondiscontinuous contours. While the CV method got trapped in local minima, like in Figs. 6(b) and (c) and 7(b), the proposed method gives very good results which confirms its robustness against initialization, and therefore its suitability to automatic systems. Comparing with the A-DLSO, the HZ method presents lower performance, for example, in Figs. 6(a) and 8(b), where it gives over-segmentation results. In many cases, the Li method also gives over segmented results, as demonstrated by Figs. 6(a) and (c) and 8(b). The GF method is less effective

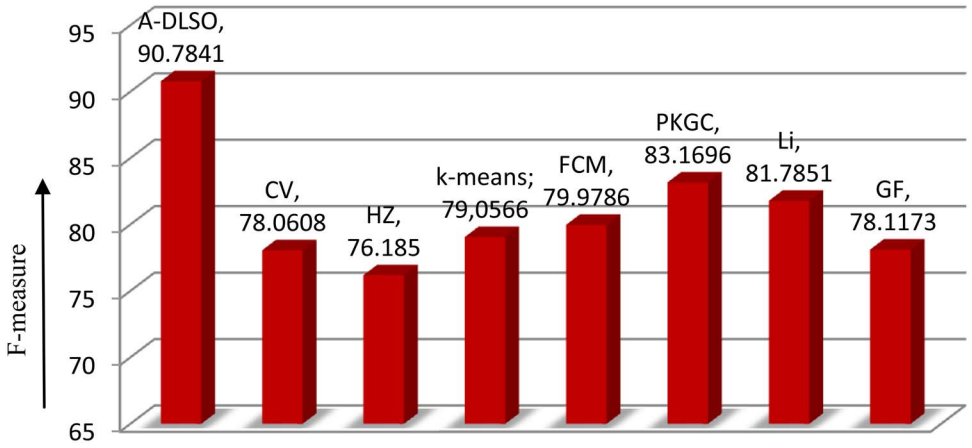

Fig. 9. 3-D histogram showing the supervised objective evaluation. The vertical axis represents the *F*-measure, while the horizontal axis represents the evaluated methods.

TABLE II
EXECUTIVE TIMES OF THE SERIAL IMPLEMENTATION ON THE CPU (IN SECOND)

Methods		**Workspace**	**Fig. 6**			**Fig. 7**			**Fig. 8**	
			(a)	**(b)**	**(c)**	**(a)**	**(b)**	**(c)**	**(a)**	**(b)**
A-DLSO	k-means	CPU	0.6468	0.4394	0.4366	0.4706	0.4631	0.6523	0.5062	0.4733
	Curve evolution		0.2146	0.2107	0.2106	0.2092	0.2108	0.2160	0.2138	0.2122
	Total		0.8614	0.6501	0.6472	0.6798	0.6739	0.8683	0.7200	0.6855
CV			85.007	84.520	85.694	84.971	84.066	85.443	137.55	84.741
HZ			0.4497	0.4508	0.4595	0.4598	0.4603	0.4575	0.4562	04541
K-means			0.6468	0.4394	0.4366	0.4706	0.4631	0.6523	0.5062	0.4733
FCM			10.214	12.614	8.4572	10.355	9.3448	12.625	8.3827	12.758
PKGC			2.6772	2.9213	2.4635	2.4909	2.4376	2.4485	2.7797	2.9501
Li			70.2741	66.8958	74.2536	50.4556	55.4759	48.6515	79.9054	56.3074
GF			0.9734	0.7701	0.7735	0.7898	0.7802	0.9750	0.8117	0.7993

TABLE III
EXECUTIVE TIMES OF THE GPU-BASED IMPLEMENTATION (IN SECOND)

Methods		**Workspace**	**Fig. 6**			**Fig. 7**			**Fig. 8**	
			(a)	**(b)**	**(c)**	**(a)**	**(b)**	**(c)**	**(a)**	**(b)**
A-DLSO	K-means	CPU	0.6468	0.4394	0.4366	0.4706	0.4631	0.6523	0.5062	0.4733
	Curve evolution	GPU	0.0204	0.0198	0.0193	0.0199	0.0202	0.0205	0.0201	0.0198
	Total		0.6672	0.4592	0.4559	0.4905	0.4833	0.6728	0.5263	0.4931
CV		GPU	47.004	46.751	47.722	46.768	46.659	47.604	62.573	46.764
HZ			0.04282	0.04334	0.04358	0.04360	0.04363	0.04318	0.04312	0.04338

than the A-DLSO, particularly when it comes to detecting steep corners, or in terms of global segmentation like in Figs. 6(b) and (c) and 7(b). In comparison with the ground-truth, the A-DLSO gives better results than the parametric kernel-based method, PKGC. As with the *k*-means clustering algorithm, the FCM and its derivatives can also be improved by our framework.

When comparing the executive times displayed by Tables II and III, we can see that even when serially implemented on the CPU, the proposed LSM is faster than almost all the methods used in these experiments. Aside from the *k*-means algorithm, only the HZ method, which uses a very simple speed function, is faster than the introduced method, but the quality of its results is far lower. The A-DLSO is far faster than the CV and the Li-based LSM. In almost all cases, it is more than one hundred times faster than the CV method, and more than eighty times faster than the Li method. A straightforward analysis of the executive times of the GPU-based implementation evinces that the curve evolution part of the introduced method has been accelerated more than ten times compared to its serial version on CPU. This is a strong proof of its suitability to massively parallel architecture. The CV

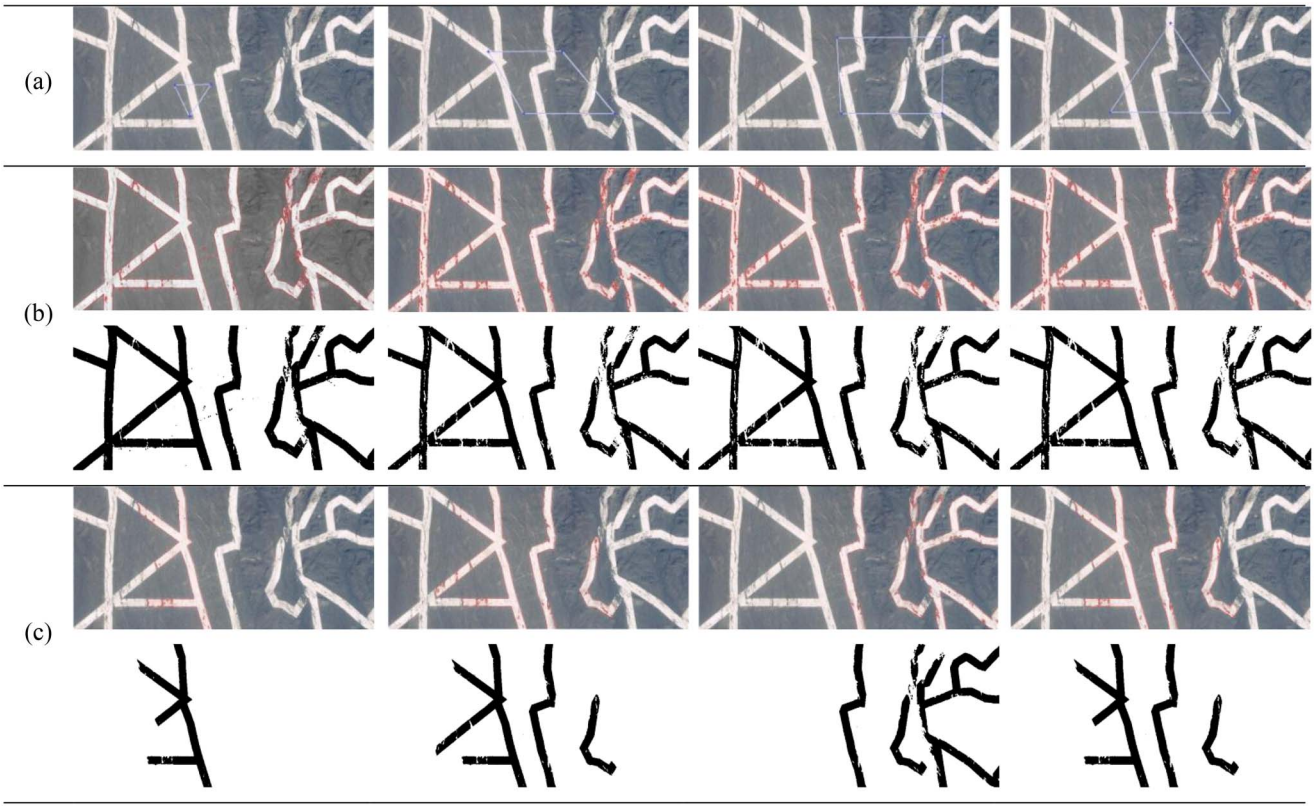

Fig. 10. Segmentation of a satellite image of Xinjiang in China with different initial contours. The results are presented in two ways, i.e., an image where the resulting contour is held on the original image, and a binary image which represents the interior of the final LSF by white pixels and the exterior by black pixels. (a) Initial contours. Results of the (b) proposed method and (c) CV method.

method which is nonlocal, because of the computation of the interior and exterior means of the active curve at each looping, has been accelerated only roughly twofold. Overall, we can conclude that the introduced A-DLSO presents very attractive performance in terms of speed comparing with level set-based models.

Fig. 10 proves the robustness of the A-DLSO to initialization. It can be seen that from different initial contours, the proposed methods quietly produces the same finally good result, while the CV method is almost always trapped into a local minimum.

V. Conclusion

This paper presents an effective and efficient level set-based image segmentation framework suitable for heterogeneous CPU–GPU architecture. The method which is also fast when serially implemented on the CPU, allows considerably improving the quality of the segmentation results obtained using most two-phase clustering algorithms such as SVM, *k*-means, FCM, and their derivatives. Thus, by combining the advantage of LSMs and clustering methods, the A-DLSO is fast, gives smooth contours with subpixel accuracy, and can easily handle complex shapes. Its robustness to initialization makes it a good candidate for automatic systems. Intensive experiments demonstrate the good performance of the proposed method.

Future works will cover an extension of the A-DLSO to multiphase image segmentation, while conserving its intrinsic locality. The memory complexity aspect will also be considered, since it is one of the limits of the LBM used to solve the proposed LSE. Furthermore, some research on A-DLSO automatic parameterization will be carried out using some machine learning techniques.

References

[1] L. Chen, C. L. P. Chen, and M. Lu, "A multiple-kernel fuzzy C-means based image segmentation," *IEEE Trans. Syst., Man, Cybern. B, Cybern.*, vol. 41, no. 5, pp. 1263–1274, Oct. 2011.

[2] H. Fu, X. Cao, Z. Tu, and D. Lin, "Symmetry constraint for foreground extraction," *IEEE Trans. Cybern.*, vol. 44, no. 5, pp. 644–654, May 2014.

[3] S. Balla-Arabé, X. Gao, and B. Wang, "A fast and robust level set method for image segmentation using fuzzy clustering and lattice Boltzmann method," *IEEE Trans. Cybern.*, vol. 43, no. 3, pp. 910–920, Jun. 2013.

[4] C. Benedek, X. Descombes, and J. Zerubia, "Building development monitoring in multitemporal remotely sensed image pairs with stochastic birth-death dynamics," *IEEE Trans. Pattern Anal. Mach. Intell.*, vol. 34, no. 1, pp. 33–50, Jan. 2012.

[5] K. Zhang, Q. Liu, H. Song, and X. Li, "A variational approach to simultaneous image segmentation and bias correction," *IEEE Trans. Cybern.*, vol. 45, no. 8, pp. 1426–1437, Aug. 2015.

[6] S. Balla-Arabé and X. Gao, "Image multi-thresholding by combining the lattice Boltzmann model and a localized level set algorithm," *Neurocomputing*, vol. 93, pp. 106–114, Sep. 2012.

[7] S. Balla-Arabé, X. Gao, B. Wang, F. Yang, and V. Brost, "Multi-kernel implicit curve evolution for selected texture regions segmentation in VHR satellite images," *IEEE Trans. Geosci. Remote Sens.*, vol. 52, no. 8, pp. 5183–5192, Aug. 2014.

[8] Y. Boycov, O. Veksler, and R. Zabih, "Fast approximate energy minimization via graph cuts," *IEEE Trans. Pattern Anal. Mach. Intell.*, vol. 23, no. 11, pp. 1222–1239, Nov. 2001.

[9] J. Malik, S. Belongie, T. Leung, and J. Shi, "Contour and texture analysis for image segmentation," *Int. J. Comput. Vis.*, vol. 43, no. 1, pp. 7–27, 2001.

[10] G. Papandreou and P. Maragos, "Multigrid geometric active contour models," *IEEE Trans. Image Process.*, vol. 16, no. 1, pp. 229–240, Jan. 2007.
[11] B. Wang, X. Gao, D. Tao, and X. Li, "A nonlinear adaptive level set for image segmentation," *IEEE Trans. Cybern.*, vol. 44, no. 3, pp. 418–428, Mar. 2014.
[12] C. Li, C.-Y. Kao, J. C. Gore, and Z. Ding, "Implicit active contours driven by local binary fitting energy," in *Proc. IEEE Conf. Comput. Vis. Pattern Recognit.*, Minneapolis, MN, USA, 2007, pp. 1–7.
[13] C. Li *et al.*, "A level set method for image segmentation in the presence of intensity inhomogeneities with application to MRI," *IEEE Trans. Image Process.*, vol. 20, no. 7, pp. 2007–2016, Jul. 2011.
[14] S. C. Zhu and A. Yuille, "Region competition: Unifying snakes, region growing, and Bayes/MDL for multiband image segmentation," *IEEE Trans. Pattern Anal. Mach. Intell.*, vol. 18, no. 9, pp. 884–900, Sep. 1996.
[15] C. C. Brun *et al.*, "A nonconservative Lagrangian framework for statistical fluid registration—SAFIRA," *IEEE Trans. Med. Imag.*, vol. 30, no. 2, pp. 184–202, Feb. 2011.
[16] A. Nakhmani and A. Tannenbaum, "Self-crossing detection and location for parametric active contours," *IEEE Trans. Image Process.*, vol. 21, no. 7, pp. 3150–3156, Jul. 2012.
[17] M. Kass, A. Witkin, and D. Terzopoulos, "Snakes: Active contour models," *Int. J. Comput. Vis.*, vol. 1, no. 4, pp. 321–331, 1988.
[18] S. Osher and J. A. Sethian, "Fronts propagating and curvature dependent speed: Algorithms based on Hamilton–Jacobi formulation," *J. Comput. Phys.*, vol. 79, no. 1, pp. 12–49, 1988.
[19] R. Malladi, J. A. Sethian, and B. C. Vemuri, "A topology-independent shape modeling scheme," in *Proc. SPIE Conf. Geom. Methods Comput. Vis. II*, vol. 2031. San Diego, CA, USA, 1993, pp. 246–258.
[20] V. Caselles, R. Kimmel, and G. Sapiro, "On geodesic active contours," *Int. J. Comput. Vis.*, vol. 22, no. 1, pp. 61–79, 1997.
[21] X. Gao, B. Wang, D. Tao, and X. Li, "A relay level set method for automatic image segmentation," *IEEE Trans. Syst., Man, Cybern. B, Cybern.*, vol. 41, no. 2, pp. 518–525, Apr. 2011.
[22] S. Kichenassamy, A. Kumar, P. Olver, A. Tannenbaum, and A. Yezzi, "Gradient flows and geometric active contours models," in *Proc. 5th Int. Conf. Comput. Vis.*, Cambridge, MA, USA, Jun. 1995, pp. 810–815.
[23] D. Cremers, M. Rousson, and R. Deriche, "A review of statistical approaches to level set segmentation: Integrating color, texture, motion and shape," *Int. J. Comput. Vis.*, vol. 72, no. 2, pp. 195–215, 2007.
[24] R. Delgado-Gonzalo, P. Thévenaz, C. S. Seelamantula, and M. Unser, "Snakes with an ellipse-reproducing property," *IEEE Trans. Image Process.*, vol. 21, no. 3, pp. 1258–1271, Mar. 2012.
[25] C. Li, C. Xu, C. Gui, and M. D. Fox, "Distance regularized level set evolution and its application to image segmentation," *IEEE Trans. Image Process.*, vol. 19, no. 12, pp. 3243–3254, Dec. 2010.
[26] S. Balla-Arabé, X. Gao, and B. Wang, "GPU accelerated edge-region based level set evolution constrained by 2D gray-scale histogram," *IEEE Trans. Image Process.*, vol. 22, no. 7, pp. 2688–2698, Jul. 2013.
[27] K. Karantzalos and D. Argiala, "A region-based level set segmentation for automatic detection of man-made objects from aerial and satellite images," *Photogramm. Eng. Remote Sens.*, vol. 75, no. 6, pp. 667–677, 2009.
[28] S. Balla-Arabé, B. Wang, and X. Gao, "Level set region based image segmentation using lattice Boltzmann method," in *Proc. 7th Int. Conf. Comput. Intell. Security*, Hainan, China, Dec. 2011, pp. 1159–1163.
[29] T. F. Chan and L. A. Vese, "Active contours without edges," *IEEE Trans. Image Process.*, vol. 10, no. 2, pp. 266–277, Feb. 2001.
[30] D. Mumford and J. Shah, "Optimal approximations by piecewise smooth functions and associated variational problems," *Commun. Pure Appl. Math.*, vol. 42, no. 5, pp. 577–685, 1989.
[31] S. Osher and R. Fedkiw, *Level Set Methods and Dynamic Implicit Surfaces*. New York, NY, USA: Springer, 2003.
[32] L. A. Vese and T. F. Chan, "A multiphase level set framework for image segmentation using the Mumford and Shah model," *Int. J. Comput. Vis.*, vol. 50, no. 3, pp. 271–293, 2002.
[33] Y. Chen *et al.*, "Using prior shapes in geometric active contours in a variational framework," *Int. J. Comput. Vis.*, vol. 50, no. 3, pp. 315–328, 2002.
[34] C. Li, C.-Y. Kao, J. C. Gore, and Z. Ding, "Minimization of region-scalable fitting energy for image segmentation," *IEEE Trans. Image Process.*, vol. 17, no. 10, pp. 1940–1949, Oct. 2008.
[35] D. Martin, C. Fowlkes, D. Tal, and J. Malik, "A database of human segmented natural images and its application to evaluating segmentation algorithms and measuring ecological statistics," in *Proc. 8th Int. Conf. Comput. Vis.*, vol. 2. Vancouver, BC, Canada, 2001, pp. 416–423.
[36] F. Gibou and R. Fedkiw, "A fast hybrid k-means level set algorithm for segmentation," in *Proc. 4th Annu. Hawaii Int. Conf. Stat. Math.*, 2005, pp. 281–291.
[37] S. Succi, *The Lattice Boltzmann Equation for Fluid Dynamics and Beyond Numerical Mathematics and Scientific Computation*. New York, NY, USA: Oxford Univ. Press, 2001.
[38] Y. Zhao, "Lattice Boltzmann based PDE solver on the GPU," *Vis. Comput.*, vol. 24, no. 5, pp. 323–333, May 2008.
[39] X. He and L.-S. Luo, "Lattice Boltzmann model for the incompressible Navier–Stokes equation," *J. Stat. Phys.*, vol. 88, nos. 3–4, pp. 927–944, 1997.
[40] P. L. Bhatnagar, E. P. Gross, and M. Krook, "A model for collision processes in gases. I. Small amplitude processes in charged and neutral one-component systems," *Phys. Rev.*, vol. 94, no. 3, pp. 511–525, 1954.
[41] J. M. Buick and C. A. Greated, "Gravity in a lattice Boltzmann model," *Phys. Rev. E*, vol. 61, no. 5, pp. 5307–5320, 2000.
[42] X. Shan and G. Doolen, "Multicomponent lattice-Boltzmann model with interparticle interaction," *J. Stat. Phys.*, vol. 81, no. 1, pp. 379–393, 1995.
[43] I. Ginzbourg and P. M. Adler, "Boundary flow condition analysis for the three-dimensional lattice Boltzmann model," *J. Phys. II*, vol. 4, no. 2, pp. 191–214, 1994.
[44] S. Chapmann and T. G. Cowling, *The Mathematical Theory of Non-Uniform Gases: An Account of the Kinetic Theory of Viscosity, Thermal Conduction and Diffusion in Gases*. Cambridge, U.K.: Cambridge Univ. Press, 1990.
[45] Y. Chen, Z. Yan, and Y. Chu, "Cellular automata based level set method for image segmentation," in *Proc. IEEE/ICME Int. Conf. Complex Med. Eng.*, Beijing, China, May 2007, pp. 171–174.
[46] G. Aubert and P. Kornprobst, *Mathematical Problems in Image Processing: Partial Differential Equations and the Calculus of Variations* (Applied Mathematical Sciences), vol. 147. New York, NY, USA: Springer, 2001.
[47] J. B. Rosen, "The gradient projection method for nonlinear programming. Part II. Nonlinear constraints," *J. Soc. Ind. Appl. Math.*, vol. 9, no. 4, pp. 514–532, 1961.
[48] S. Wang and X. Yao, "Relationships between diversity of classification ensembles and single-class performance measures," *IEEE Trans. Knowl. Data Eng.*, vol. 25, no. 1, pp. 206–219, Jan. 2013.
[49] H. He and E. A. Garcia, "Learning from imbalanced data," *IEEE Trans. Knowl. Data Eng.*, vol. 21, no. 9, pp. 1263–1284, Sep. 2009.
[50] M. B. Salah, A. Mitiche, and I. B. Ayed, "Multiregion image segmentation by parametric kernel graph cuts," *IEEE Trans. Image Process.*, vol. 20, no. 2, pp. 545–557, Feb. 2011.
[51] A. Hagan and Y. Zhao, "Parallel 3D image segmentation of large data sets on a GPU cluster," in *Proc. 5th Int. Symp. Visual Comput.*, Las Vegas, NV, USA, 2009, pp. 960–969.
[52] Y. Bazi, F. Melgani, and H. D. Al-Sharari, "Unsupervised change detection in multispectral remotely sensed imagery with level set methods," *IEEE Trans. Geosci. Remote Sens.*, vol. 48, no. 8, pp. 3178–3187, Aug. 2010.

Souleymane Balla-Arabé (M'12) received the M.Eng. degree in electronic from Polytechnic Military School, Algiers, Algeria, in 2004, and the Ph.D. degree in information and communication engineering from Xidian University, Xi'an, China, in 2014.

He is currently a Research Fellow with the Laboratory of Electronic, Computing and Imaging Sciences CNRS-UMR 6306, University of Burgundy, Dijon, France. His current research interests include architecture-aware optimization strategies for image segmentation, graphics processing unit-based computations, computational intelligence, machine learning, and computer vision. He has published several technical articles in refereed journals and proceedings, including the IEEE TRANSACTIONS ON IMAGE PROCESSING, the IEEE TRANSACTIONS ON GEOSCIENCE AND REMOTE SENSING, and the IEEE TRANSACTIONS ON CYBERNETICS in the above areas.

Xinbo Gao (M'02–SM'07) received the B.Eng., M.Sc., and Ph.D. degrees in signal and information processing from Xidian University, Xi'an, China, in 1994, 1997, and 1999, respectively.

From 1997 to 1998, he was a Research Fellow with the Department of Computer Science, Shizuoka University, Shizuoka, Japan. From 2000 to 2001, he was a Post-Doctoral Research Fellow with the Department of Information Engineering, Chinese University of Hong Kong, Hong Kong. Since 2001, he has been with the School of Electronic Engineering, Xidian University. He is currently a Cheung Kong Professor with the Ministry of Education, a Professor of Pattern Recognition and Intelligent System, and the Director of the State Key Laboratory of Integrated Services Networks, Xi'an. He has published five books and around 200 technical articles in refereed journals and proceedings. His current research interests include multimedia analysis, computer vision, pattern recognition, machine learning, and wireless communications.

Prof. Gao served as the General Chair/Co-Chair, the Program Committee Chair/Co-Chair, or a PC Member for around 30 major international conferences. He is on the Editorial Board of several journals, including *Signal Processing* (Elsevier) and *Neurocomputing* (Elsevier). He is currently a fellow of the Institution of Engineering and Technology.

Dominique Ginhac (M'15) received the master's degree in engineering and the Ph.D. degree in computer vision from Blaise Pascal University, Clermont-Ferrand, France, in 1995 and 1999, respectively.

He joined the University of Burgundy, Dijon, France, in 2000 and became a member of the Laboratory of Electronic, Computing and Imaging Sciences (LE2I) CNRS-UMR 6306. In 2009, he was promoted as a Professor and became the Head of the Electrical Engineering Department until 2011. He is currently a Deputy Director of the LE2I. His current research interests include rapid prototyping of real-time image processing on dedicated parallel architectures, image acquisition, hardware design of smart vision systems, and implementation of real-time image processing applications.

Vincent Brost received the M.S. degree in electrical engineering and the Ph.D. degree in image processing and electrical engineering from the University of Burgundy, Dijon, France, in 2000 and 2006, respectively.

He is currently an Associate Professor with the University of Burgundy and a member of the Laboratory of Electronic, Computing and Imaging Sciences CNRS-UMR 6306. His current research interests include rapid prototyping system, very long instruction word architecture, and electronic devices.

Fan Yang was born in Tianjin, China, in 1963. She received the B.S. degree in electrical engineering from the University of Lanzhou, Lanzhou, China, in 1982, and the M.S. degree in computer science and the Ph.D. degree in image processing from the University of Burgundy, Dijon, France, in 1994 and 1998, respectively.

She is currently a Full Professor and a member of the Laboratory of Electronic, Computing and Imaging Sciences CNRS-UMR 6306, University of Burgundy. Her current research interests include patterns recognition, neural network, motion estimation based on spatial-temporal Gabor filters, parallelism and real-time implementation, and biometric image processing algorithms and architectures.

Prof. Yang is a member of the French Research Group Information, Signal, Images, and Vision. She livens up the Theme C: Algorithm Architecture Mapping.